Side-Chain Effect on the Structural Evolution and Properties of Poly(9,9-dihexylfluorene-*alt*-2,5-dialkoxybenzene) Copolymers

Gui-Zhong Yang, Wei-Zhi Wang, Min Wang, and Tianxi Liu*

Key Laboratory of Molecular Engineering of Polymers of Ministry of Education, Department of Macromolecular Science, Laboratory of Advanced Materials, Fudan University, Shanghai 200433, People's Republic of China

Received: January 19, 2007; In Final Form: May 14, 2007

The structural evolution and properties of poly(9,9-dihexylfluorene-*alt*-2,5-dialkoxybenzene) with different lengths of alkoxy side chains on phenylene have been systematically investigated by means of thermogravimetric analysis (TGA), X-ray diffraction (XRD), differential scanning calorimetry (DSC), polarizing light microscopy (PLM), atomic force microscopy (AFM), and cyclic voltammetry (CV) techniques. The polymer self-organizes into a lamellar structure consisting of both two- and one-layer packing, and the two-layer packing style is the dominant structure. In addition, the two-layer and one-layer packing structures also accompany the presence of planar stacking and/or crystalline and noncrystalline structures, thus maintaining the stability of the packing. PF6OC6 shows three ordered phases (two crystalline phases and one nematic phase) during the heating process. With further increase of the length of alkoxy side chains, only two ordered phases (one crystalline phase and one nematic phase) are observed and the polymers show a melting−recrystallization phenomenon, which is steadily inhibited as the length of the alkoxy side chains increases. The optical and electrochemical properties of the polymers do not exhibit noticeable dependence on the length of the alkoxy side chains. However, the thermal stability, the vibronic structures, and the full width at half-maximum (fwhm) in photoluminescence spectra of the films gradually decrease, and the oxidation onset potentials and the corresponding HOMO energy levels slightly increase with increasing length of alkoxy side chains on phenylene. These results indicate that the length variation of alkoxy side chains does not change the electronic structure of the polymer backbones, but remarkably affects the microphase separation between the flexible side chains and the conjugated backbones.

Introduction

Polymers or oligomers containing a fully π-conjugated backbone are a novel class of functional materials that have attracted extensive attention from researchers in materials chemistry and device physics. It has been noted that the functionality of these materials depends on the physical structures of the polymers or oligomers from single molecules to condensed state. The most typical examples include some conjugated oligomers or small molecules with highly ordered structures. Additionally, some studies show evidence that many luminescent polymers are highly emissive in their dilute solution but become weakly luminescent when fabricated into thin solid films. The loss or reduction of luminescence is due to aggregation of polymer chains by producing a strong chain interaction and thus an excitation−excitation annihilation. However, the investigations concerning the so-called chain aggregation in the solid state are essentially lacking. Therefore, a fundamental understanding of the physical structures or supramolecular morphology (closely related to the aggregation) of these materials is of great significance to maximize the material functionality by simply manipulating their supramolecular structures.

Conjugated polymers, such as polyfluorenes (PFs),[1−7] polythiophenes (PTs),[8−11] poly(*p*-phenylene)s (PPPs),[12−14] and their derivatives have been extensively studied in the past decade due to their potential applications in various optoelectronic devices. In general, conjugated polymers have poor solubility in most organic solvents before being modified with flexible side chains. The introduction of flexible side chains such as alkyl or alkoxy onto the main-chain backbone not only improves the solubility and film-forming characteristics, but also confers new functionality and alters the supramolecular structure at nanoscales for these conjugated polymers.[15−17] Usually, the polymers consisting of rigid backbones and flexible side chains are called hairy-rod polymers, which tend to self-organize and form nanostructures in bulk or in solution, due to microphase separation between the flexible side chains and the rigid backbones. The nature and length of the flexible side chains have obvious effects on the phase behavior of hairy-rod polymers.[18] In addition, the variety of phase behavior also depends on the selection of the backbones and the side chains.

PPPs,[19−22] PTs,[23] and PFs[14] substituted with a variety of flexible groups have attracted much attention. Poly(2,5-didodecyl-1,4-phenylene) can self-organize and form a lamellar structure with a long period of about 3.5 nm at room temperature. The long period disappears when it is heated to about 190 °C.[19] When the alkyl side chains are replaced by alkoxy side chains, the self-organized lamellar structure can be obtained for the polymers substituted with octyloxy and dodecyloxy side chains. However, for shorter butoxy or pentoxy substitution, the self-organized structure of the polymers is approximately cylindrical because these side chains are too short to induce microphase separation.[20] For poly(3-alkylthiophene)s, as the carbon number of alkyl group is up to 4, the self-organized

* Corresponding author. Telephone: +86 21 55664197. Fax: +86 21 55664192. E-mail: txliu@fudan.edu.cn.

10.1021/jp0704620 CCC: $37.00
Published on Web 06/16/2007

SCHEME 1: Chemical Structure of the Polymers

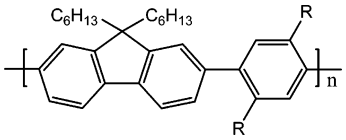

R = OC_6H_{13} **PF6OC6**
OC_8H_{17} **PF6OC8**
$OC_{10}H_{21}$ **PF6OC10**
$OC_{12}H_{25}$ **PF6OC12**

lamellar structures are obtained.[23] Furthermore, the X-ray diffraction results suggest the presence of a two-layer structure and a one-layer structure for the packing of side chains, and the polymer mainly forms the two-layer structure in ordered phase.[23] Recently, the morphology and phase behavior of poly(9,9-dialkylfluorene)s have been systemically investigated.[24−27] Poly(9,9-dihexylfluorene) (PFH) and poly(9,9-dioctylfluorene) (PFO) as homologues have qualitative similarities in phase behavior. They exhibit an intrinsic metastability of lamellar (β) mesomorph in the as-cast films, nematic liquid crystal at high temperatures, and two crystalline (α and α') polymorphs in the solid state. Both PFH and PFO also have a qualitative difference. For PFH, the β phase as major crystalline precursor could not be identified and it might persist up to a much higher temperature of about 250 °C. However, for PFO, the β phase was a degenerated form of a crystalline clathrate phase that appeared in the early stage of film formation and was easily dissipated around 100 °C.[24−27]

As for PF and/or PPP derivatives, the photophysical properties of fluorene-*alt*-benzene based copolymers have been extensively investigated by attaching different side groups on phenylene.[28−31] They exhibit very high photoluminescence quantum efficiency and excellent thermal stability. However, to our knowledge, structural investigations on the fluorene-*alt*-benzene based copolymers are still lacking. In this paper, the side-chain effect on the structural evolution and properties of poly(9,9-dihexylfluorene-*alt*-2,5-dialkoxybenzene) is systemically studied.

Experimental Section

The polymers used here were synthesized through a Suzuki coupling reaction in our previous paper,[31] and the chemical structures are shown in Scheme 1. These polymers are readily dissolved in common organic solvents, such as chloroform and xylene at room temperature, due to the attachment of long side chains onto the rigid backbones. From the viewpoint of main-chain conformation, these stiff polymers are important members of the shape-persistent macromolecules (SPMs) family[32] featuring a persistent chain trajectory, i.e., a highly geometrically anisotropic shape. The molecular weights of the polymers shown in Table 1 were determined by gel permeation chromatography (GPC) using polystyrene as the standard.

Thermogravimetric analysis (TGA) was conducted on a Shimadzu DTG-60H under a heating rate of 10 °C/min in air and nitrogen atmosphere. Differential scanning calorimetry (DSC) was performed on a Shimadzu DSC-60A at a heating and cooling rate of 10 °C/min in nitrogen atmosphere. The instrument was calibrated with high-purity indium and zinc.

X-ray diffraction (XRD) measurements were carried out at room temperature using a Bruker Nanostar U System, with incident X-ray wavelength ($\lambda = 0.1542$ nm). The collimation system consists of two cross-coupled Gobel mirrors and four pinholes. A Histar 2D area detector (Siemens) filled with pressurized xenon gas was used to record the one-dimensional (1D) XRD patterns at a voltage of 40 kV and a current of 40 mA.

Atomic force microscopy (AFM) was performed under tapping mode on a Digital Instruments Nanoscope IV (Veeco Instruments, Santa Barbara, CA) equipped with a silicon cantilever with 125 μm and an E-type vertical engage piezoelectric scanner. The samples were prepared by dropping the xylene solution on freshly cleaved mica and then drying naturally at room temperature. Polarizing light microscopy (PLM) measurements were carried out on an Olympus polarizing light microscope (BX51) with a hot stage.

Fluorescence measurements were carried out on a Shimadzu RF-5301 PC spectrofluorometer with a xenon lamp as a light source. Photoluminescence quantum efficiency (PLQE) measurements of the films were made using a calibrated integrating sphere coupled via an optical fiber linked to a scanning monochromator with a photomultiplier detector. The samples were excited with a 374 nm Zolix PHLM-2 laser.

Cyclic voltammetry (CV) experiments were performed in a solution of tetrabutylammonium hexafluorophosphate ($TBAPF_6$) (0.1 M) in acetonitrile at a scan rate of 100 mV/s at room temperature under the protection of nitrogen. A glassy carbon electrode coated with a thin polymer film was used as the working electrode. A Pt wire was used as the counter electrode, and an $Ag/AgNO_3$ electrode was used as the reference electrode.

Results and Discussion

Thermogravimetric Analysis. The thermal stability of the polymers is evaluated using thermogravimetric analysis. Table 1 shows the decomposition temperature (T_d) (at 5% weight loss) of the polymers in both air and nitrogen atmospheres. It can be seen that the four polymers exhibit good thermal stability. Their decomposition starts at ca. 380 °C in nitrogen atmosphere and ca. 370 °C in air, respectively. Since the flexible (aliphatic) alkoxy side chains are structurally easy to decompose or oxidize upon thermal treatment, the values of T_d steadily decrease with increasing length of side chains on phenylene in both atmospheres, which may be attributed to the increase of the relative weight fraction of the flexible side chains as the length of the side chains increases. That is, the increase of side chain length reduces the thermal stability of the polymers. As expected, the values of T_d in air are lower than those in nitrogen atmosphere.

Morphology. Theoretical treatments of the self-organized structure formation of hairy-rod polymers predict that nematic, lamellar, and hexagonal microphase separated structures as well as isotropic phase are typically present with varying structure parameter of the hairy-rod polymers.[18] In order to understand the microphase structure of poly(9,9-dihexylfluorene-*alt*-2,5-dialkoxybenzene), XRD technique was employed. Figure 1 shows one-dimensional XRD patterns of the powdery polymer

TABLE 1: Molecular Weight and Thermogravimetric Analysis Data of the Polymers

				T_d (°C)	
polymer	M_n	M_w	M_w/M_n	in air	in N_2
PF6POC6	17 500	28 000	1.60	392.5	404.8
PF6POC8	22 300	39 900	1.79	386.9	396.3
PF6POC10	29 400	53 800	1.83	380.4	387.8
PF6POC12	20 000	36 200	1.81	372.3	380.9

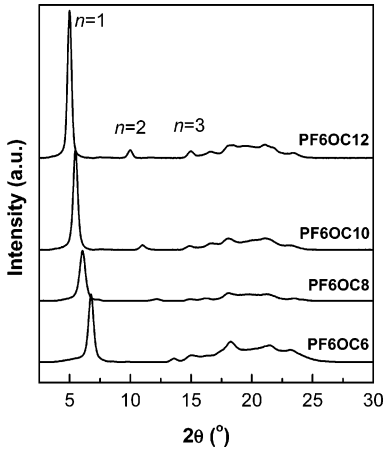

Figure 1. XRD patterns of the polymers.

samples, and Figure 2 is the corresponding two-dimensional XRD patterns. For PF6OC6, a high-intensity diffraction peak ($n = 1$) and several weak diffraction peaks ($n = 2, 3, 4, ...$) are observed. The d spacing determined from the $n = 1$ and $n = 2$ reflections are 13.1 and 6.5 Å, respectively, suggesting a periodic lamellar structure with the main chains separated by the side chains. That is, the space between the two neighboring coplanar subchains on the same plane is filled with the side chains. The presence of $n = 2$ reflection indicates a higher ordering degree of space filling of the alkoxy side chains. The lamellar structure is commonly found in PATs,[33] poly(3,4-ethylenedioxythiophene),[34] supramolecular polypyridine,[35,36] or polyphenylene,[37] and other hairy-rod polymers. Generally, formation of the lamellar phase of π-conjugated hairy-rod polymers is driven by stacking of the backbone rings and side-chain crystallization.[38] The lamellar phase thus arises mostly from sufficiently planar molecules, such as poly(3-hexylthiophene).[39] When the length of alkoxy side chains on phenylene increases, similar results are obtained for PF6OC8, PF6OC10, and PF6OC12. The lamellar structures of the polymers are proposed as shown in Figure 3 according to the XRD results. On examination of the $n = 1$ reflection, the corresponding d spacings are found to increase with increasing length of the side chains on phenylene ($d = 14.5$ Å for PF6OC8, $d = 16.1$ Å for PF6OC10, and $d = 17.7$ Å for PF6OC12). The same trend is also observed for the $n = 2$ reflections of the polymers. However, for the $n = 3$ and other higher order reflections of all the polymers studied here, the corresponding d spacings are 5.9, 5.4, 4.9, 4.4, 4.1, and 3.8 Å for $n = 3$, 4, 5, 6, 7, and 8 reflections, respectively. This side-chain-length independence of the d spacing may be assigned to two aspects. One may be the spacing between two successive stacking planes of coplanar subchains (or intraplanar spacing) as shown in Figure 3c,d. Another may be involving a more complex noncrystalline and crystalline phase structure due to side-chain interplay. Plots of the d spacing of the $n = 1$, 2, and 3 reflections versus the number of carbon atoms of side chain on phenylene give a series of straight lines, as shown in Figure 4. The d spacing corresponding to the $n = 1$ reflection indicates the formation of an interdigitated two-layer packing, as shown in Figure 3a. For the d spacing corresponding to the $n = 2$ reflection, its value is almost exactly half that of the $n = 1$ reflection. This indicates an existence of one-layer packing, which is probably formed by intercalation of the extended or torsional side chains between two neighboring coplanar subchains, as shown in Figure 3b. Obviously, the two- and one-layer packings coexist in the supramolecular structure of poly(9,9-dihexylfluorene-*alt*-2,5-dialkoxybenzene), and the fraction of the two-layer packing is much higher than that of

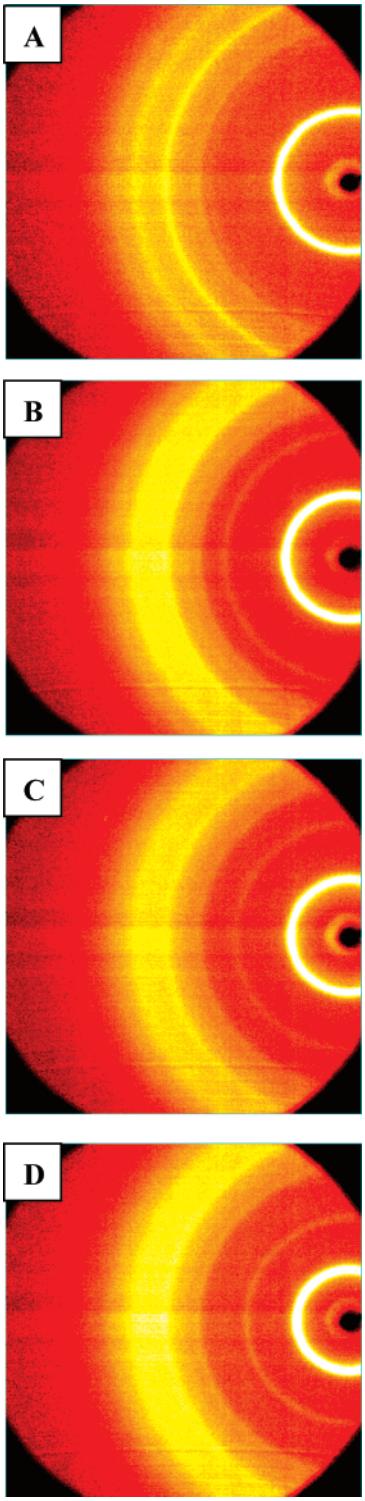

Figure 2. Two-dimensional X-ray diffraction patterns of PF6OC6 (A), PF6OC8 (B), PF6OC10 (C), and PF6OC12 (D).

the one-layer packing, because the diffraction intensity of the $n = 1$ reflection is much higher than that of the $n = 2$ reflection. In addition, the two- and one-layer packings also accompany the presence of planar stacking and/or crystalline and noncrystalline structures due to the presence of other higher order reflections, thus maintaining the stability of the packing structure. Similar observations were also reported for other hairy-rod polymers with flexible side chains, such as poly(3-alkylthiophene)s[23,39] and poly(2,5-dialkyl-1,4-phenylene)s.[19]

The self-assembled morphology of solvent-cast deposits of the polymers from xylene was investigated using AFM. Figure

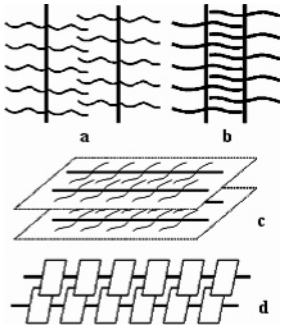

Figure 3. Schematic diagram of the layer structure of the polymers: (a) ordered two-layer structure, (b) ordered single-layer structure, and (c) and (d) planar packing.

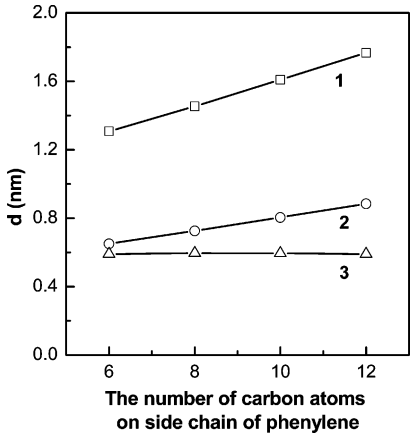

Figure 4. Plots of the *d* spacing of $n = 1$, 2, and 3 reflections from the XRD patterns versus number of carbon atoms of alkoxy side chains on phenylene.

5 shows the AFM images of PF6OC6 and PF6OC8. Very interestingly, numerous and randomly oriented wormlike lamellae are observed with two tapered heads. This typical morphological feature has been previously observed in the thin films solidified from the lyotropic phase of another SPM, polydiacetylene.[40] It probably suggests that the liquid crystalline nature of these SPMs allows the rigid molecules to self-assemble into highly ordered structures. The average thickness of the lamellae is in the range of 50−70 nm, and the lamellae at the head areas are especially much thinner. The chain ends or other structural defects are probably accumulated in the areas between the lamellae; thus the packing density in these areas is lower than that in lamellar areas. The wormlike or fibrillar morphology was clearly observed in both height and phase signals across the entire area of the scan. The so-called hairy-rod polymers generally self-organize into fibrillar morphology and were previously reported in conjugated polymers such as poly(3-alkylthiophenes),[11] poly(9,9-dialkylfluorene),[6] and fluorene-*alt*-benzene copolymers[30] because of microphase separation between the rigid backbone and the flexible side chains.

Phase Behavior. Most fluorene-based conjugated polymers usually show interesting liquid crystalline features, which have found potential applications in polarized light emission.[7] Here, the phase behavior is investigated as a function of side-chain length using DSC and XRD techniques. The DSC thermograms of the four polymers are shown in Figure 6. The samples for XRD measurements were first heated to 250 °C for 5 min and cooled to room temperature, then annealed at the indicated temperature in nitrogen atmosphere for 30 min, and finally quenched in liquid nitrogen.

For PF6OC6, two endothermic peaks at about 129 and 142 °C are observed in the first heating run (Figure 6A). In the

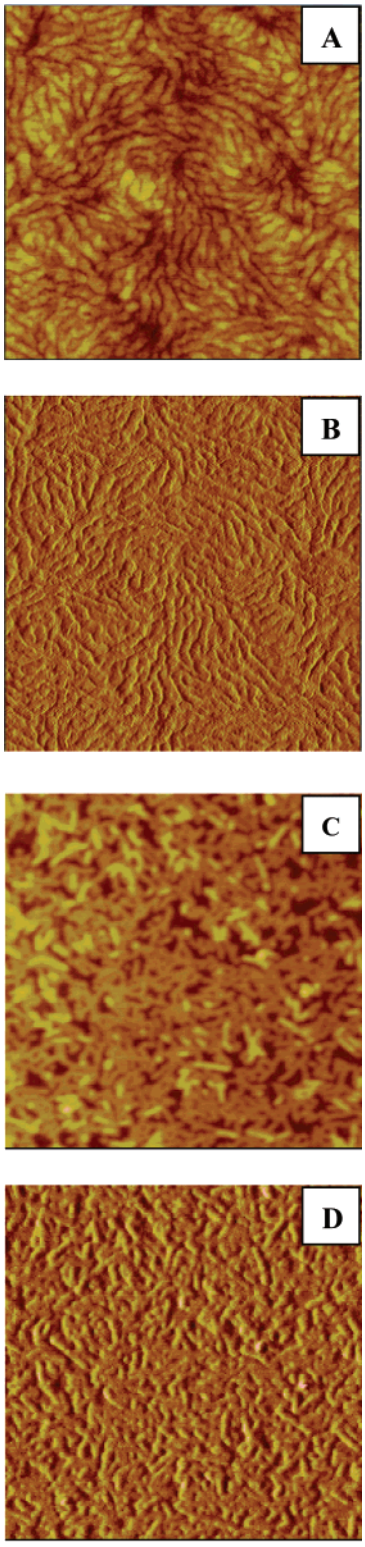

Figure 5. AFM images (2 μm × 2 μm) of the films for PF6OC6 (A, B) and PF6OC8 (C, D). (A) and (C) are height images; (B) and (D) are the corresponding phase images.

cooling run, it does not show any phase transition (Figure 6B). However, in the second heating run a new exothermic peak at about 115 °C is observed just prior to the endothermic peak at 129 °C (Figure 6C). In addition, a weak step drop is observed at about 65 °C, which is assigned to the glass transition. Obviously, the phase transition behavior of PF6OC6 is very interesting. In order to investigate the phase behavior of PF6OC6, the XRD measurements were carried out with the

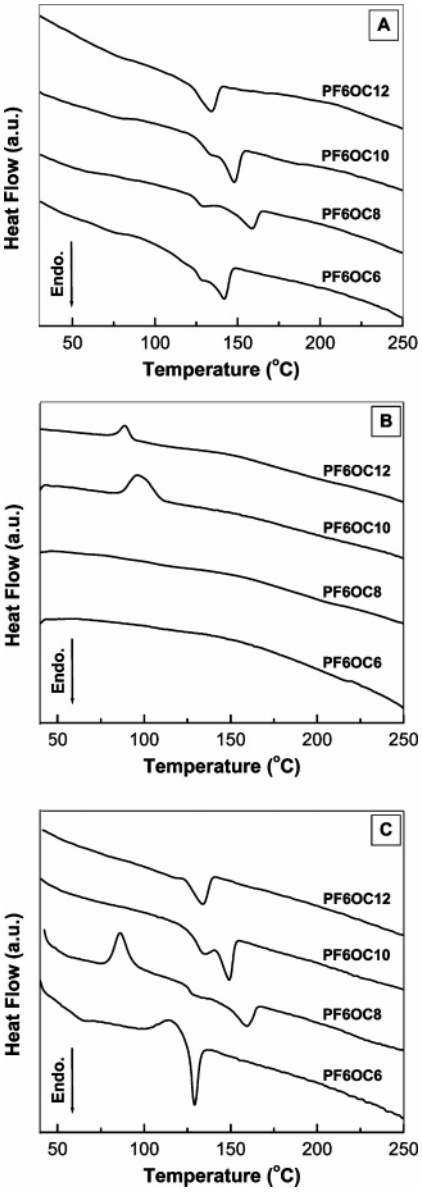

Figure 6. DSC thermograms of the polymers: (A) the first heating scan, (B) the cooling scan, and (C) the second heating scan. Heating and cooling rate: 10 °C/min.

samples annealed at different temperatures and the resultant XRD patterns are shown in Figure 7. For comparison, the corresponding hot-stage polarizing light microscopy (PLM) images of PF6OC6 at different temperatures are shown in Figure 8. It can be seen that PF6OC6 exhibits a characteristic nematic liquid crystalline phase above about 142 °C (Figure 8E), and the nematic phase still exists even after starting decomposition (Figure 6F). Therefore, the temperature (ca. 142 °C) is attributed to the nematic liquid crystalline phase transition temperature. Besides the $n = 1$ reflection at low scattering angle, Figure 7 shows a new diffraction peak at $2\theta = 5.45°$ for the samples annealed at 53, 70, and 130 °C, indicating the appearance of a new phase. In addition, the XRD patterns for the samples annealed at 95 and 115 °C are consistent with those for the powdery samples (Figure 1). Thus, the endothermic peak (at ca. 129 °C) can be assigned to the transition from one crystalline phase (C1) to another one (C2). The XRD results of the samples annealed at 53, 70, and 95 °C further confirm that the transition between the two crystalline phases is reversible. The exothermic peak (at ca. 115 °C) in Figure 6C corresponds to a recrystal-

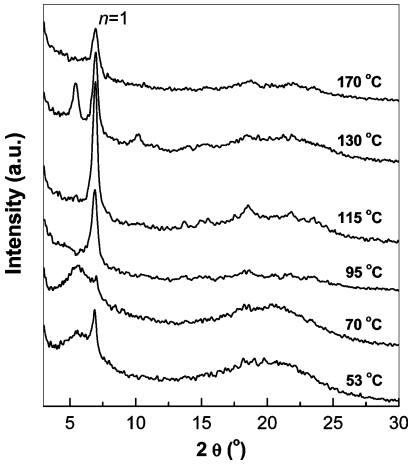

Figure 7. XRD patterns of PF6OC6 samples which were first heated to 250 °C for 5 min and cooled to room temperature, and then annealed at the indicated temperature for 30 min in nitrogen atmosphere and finally quenched in liquid nitrogen.

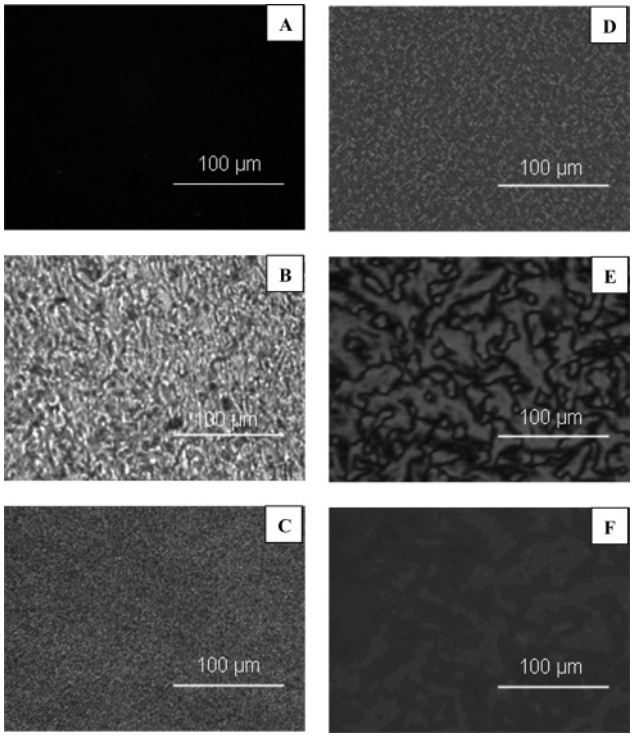

Figure 8. Polarized light microscopy (PLM) images (×500) of PF6OC6 films at different temperatures: (A) pristine films, (B) sample first heated to 250 °C and then cooled to room temperature; (C) sample at 110 °C, (D) sample at 130 °C, (E) sample at 150 °C, and (F) sample at 400 °C.

lization process. The nematic phase transition (at ca. 142 °C) is not observed in the second heating run, probably due to coexistence of the nematic phase (N) and the C2 phase after the cooling run thus making it difficult to detect the enthalpy of the phase transition by DSC. The coexistence of the nematic phase with the crystalline phases is also confirmed using PLM observation (Figure 8B). In addition, the pristine film was amorphous (Figure 8A). The phase behavior of PF6OC6 at 110 °C (Figure 8C) and that at 130 °C (Figure 8D), corresponding to C1 and C2, respectively, showed discernible difference from each other.

Similar to PF6OC6, two endothermic peaks at about 129 and 160 °C are observed for PF6OC8 in the first heating scan (Figure 6A), and no any phase transition was observed in the cooling

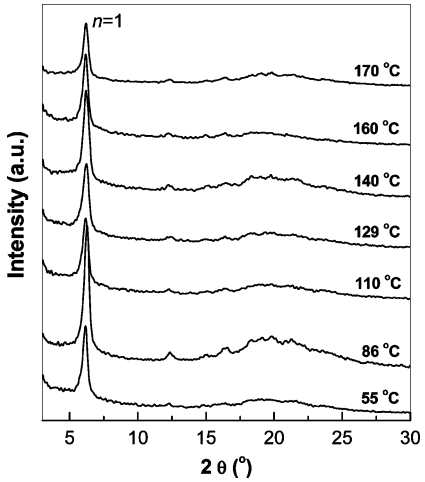

Figure 9. XRD patterns of PF6OC8 samples thermally treated as in Figure 7 for PF6OC6.

scan (Figure 6B). However, for the second heating (Figure 6C) the endothermic peak at ca. 160 °C is still observed in addition to a new exothermic peak at about 86 °C and an endothermic peak at ca. 129 °C. The difference between the two polymers (i.e., PF6OC6 and PF6OC8) is only two carbon atoms of the side chains on phenylene. Moreover, the XRD patterns of the PF6OC8 annealed at different temperatures shown in Figure 9 are identical to that in Figure 1, indicating that only one crystalline structure exists for PF6OC8. The PLM images of PF6OC8 at different temperatures are shown in Figure 10. PF6OC8 also exhibits a characteristic nematic liquid crystalline phase above 160 °C (Figure 10D). And after the film was cooled from 250 °C to room temperature, PLM observation showed a coexistent morphology of the nematic phase and the crystalline phase (Figure 10A). The dark areas mainly consist of nematic phase, and the bright areas are the crystalline phase, indicating that the crystal size is very small. As the temperature of the hot stage increases, the fraction of nematic phase steadily decreases and transforms into crystalline phase, resulting in formation of closely stacked crystals, as shown in Figure 10B. However, the crystals first partly melt and then gradually grow with further increasing temperature (Figure 10C), and finally change into the nematic phase above about 160 °C (Figure 10D). Thus, the exothermic peak at ca. 86 °C can be attributed to a recrystallization process, the first endothermic peak at ca. 129 °C corresponds to a melting−recrystallization process, and the second endothermic peak at ca. 160 °C can be assigned to the transition from the crystalline phase to the nematic phase.

When the length of side chain on phenylene increases from octyloxy (PF6OC8) to decyloxy (PF6OC10), the phase behavior of PF6OC10 is very similar to that of PF6OC8. Two endothermic peaks at about 134 and 148 °C are observed during both the first and the second heating runs (Figure 6A,C). The main difference is that the recrystallization peak at ca. 95 °C appears in the cooling run for PF6OC10 (Figure 6B), while for PF6OC8 the recrystallization peak appears in the second heating run (Figure 6C). Thus, combining the DSC results with the XRD patterns (Figure 11A), the first endothermic peak (at ca. 134 °C) can be attributed to a melting−recrystallization process, and the second one (at ca. 148 °C) corresponds to a nematic phase transition (Figure 12A), as discussed above for the case of PF6OC8.

When further increasing the side-chain length on phenylene, i.e., for the case of PF6OC12, more interesting results are obtained. During the first and second heating scans, only one

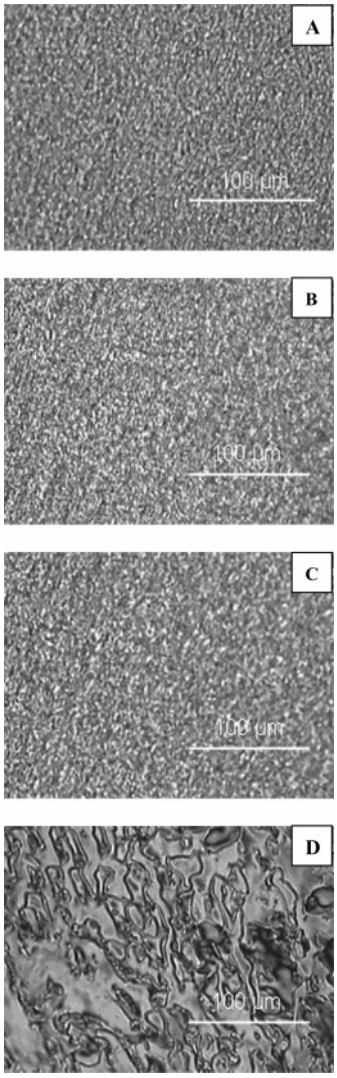

Figure 10. Polarized light microscopy (PLM) images (×500) of the PF6OC8 films at different temperatures: (A) the sample first heated to 250 °C and then cooled to room temperature, (B) sample at 86 °C, (C) sample at 140 °C, and (D) sample at 170 °C.

endothermic peak at about 134 °C is observed (Figure 6A,C). The cooling scan (Figure 6B) also shows a recrystallization peak at about 88 °C. The endothermic peak can be assigned to a nematic phase transition, by combining the DSC data with the XRD results (Figure 11B) and the hot-stage PLM observation (inset of Figure 12B).

The phase behavior of these polymers exhibits obviously the dependence on the side-chain length on phenylene, indicating that microphase separation between the alkoxy side chains and the conjugated backbones varies with increasing the length of the alkoxy side chains on phenylene. For PF6OC6, three ordered phases (two crystalline phases and one nematic phase) were observed. However, on increasing the side-chain length from hexyloxy (PF6OC6) to octyloxy (PF6OC8), decyloxy (PF6OC10), and dodecyloxy (PF6OC12), only two ordered phases (one crystalline phase and one nematic phase) were observed. Such variation of the phase behavior can be attributed to the increase of microphase separation between the flexible side chains and the conjugated rigid backbones as well as the existing intermolecular and intramolecular entwisting with increasing side-chain length. Although the phase structures of PF6OC8, PF6OC10, and PF6OC12 are similar, their phase behaviors still show obvious variation with increasing side-chain length. On

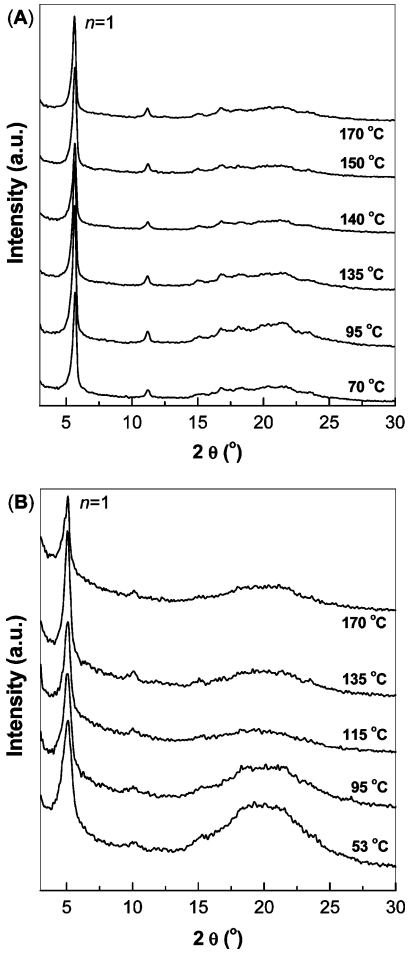

Figure 11. XRD patterns of PF6OC10 film (A) and PF6OC12 film (B). The samples were thermally treated as in Figure 7 for PF6OC6.

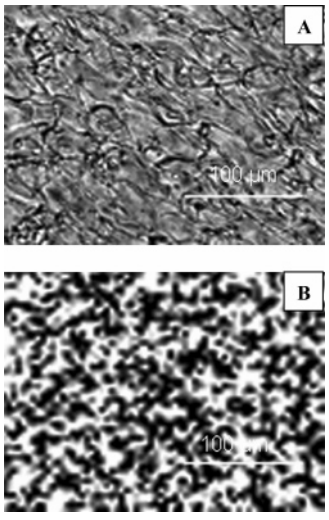

Figure 12. Polarized light microscopy (PLM) images (×500) of PF6OC10 (A) and PF6OC12 (B) at 170 °C.

the one hand, the liquid crystalline phase transition temperature gradually decreases as the side-chain length increases. On the other hand, the melting−recrystallization behavior can be observed except for PF6OC12, and the interval between the two endothermic peaks decreases with increasing the side-chain length on phenylene. It is interesting to note that the melting−recrystallization behavior is greatly inhibited as the side-chain length increases. This is probably because melt crystallization is a diffusion control process. The intermolecular and/or

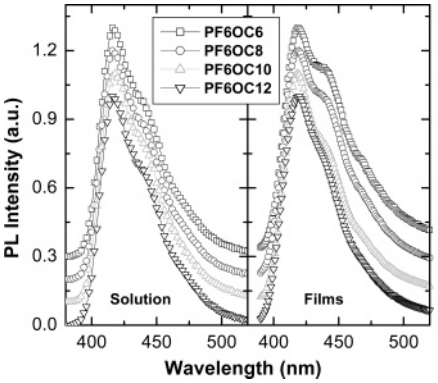

Figure 13. PL spectra of the polymers in chloroform solution (10^{-5} M) and the pristine films.

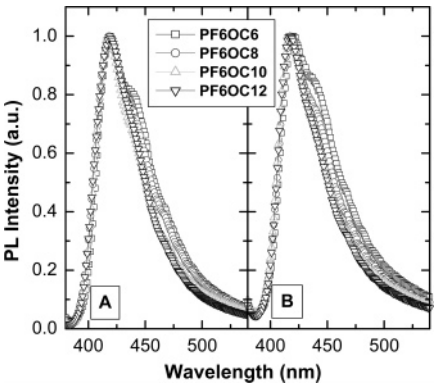

Figure 14. PL spectra of the polymer films annealed at 80 (A) and 200 °C (B) for 1 h in air.

intramolecular interactions steadily increase with the increase of the side-chain length, indicating the longer side-chain sample with the lower diffusivity. Thus the melting−recrystallization phenomenon can be effectively prohibited for the polymer with longer side chains.

The origin of the morphological complexity in the SPMs probably comes from the particular chemical structures, i.e., long and flexible side chains chemically attached to the rigid backbones of the SPMs, giving rising to a structural variety from chemical structure to chain rigidity and to structural geometry.[41]

Optical Properties. The absorption spectra of the four polymers do not show noticeable differences in spectral shape from each other, and their absorption maxima for chloroform solutions and the films are shown in Table 2. They exhibit the identical absorption maximum at 370 nm for the chloroform solutions and at 382 nm for the films. The absorption spectra do not exhibit dependence on the length of alkoxy side chains, indicating that the variation of the length of alkoxy side chains on phenylene does not change the electronic structure of the backbone of the polymers. The spectral red shift from the solutions to the films can be attributed to the formation of chain aggregation. The identical phenomenon is also observed for their photoluminescence (PL) spectra with maximum at 415 nm for the solutions and 420 nm for the films (Figure 13). On the one hand, however, the vibronic structures (i.e., the discernible shoulder peak at ca. 440 nm) and the full width at the half-maximum (fwhm) in the PL spectrum gradually decrease for the film samples (Table 2), but show almost no variation for the solution samples with increasing length of the alkoxy side chains on phenylene. On the other hand, the amount of the vibronic structures decreases when changing from the film to the solution. The dependence of the vibronic structures and the

TABLE 2: Optical Properties of the Polymers

	solution λ_{max} (nm)			film λ_{max} (nm)			PLQE (%)	
polymer	abs	em	fwhm	abs	em	fwhm	solution	film
PF6POC6	370	415	44.98	382	420	52.57	49.2	40.9
PF6POC8	370	415	44.96	382	420	50.84	49.7	40.5
PF6POC10	370	415	44.97	382	420	46.73	49.5	41.0
PF6POC12	370	414	44.98	382	420	45.31	50.1	40.0

TABLE 3: Electrochemical Properties of the Polymers

		cyclic voltammetry				
polymer	UV−vis band gap (eV)	$E_{onset/Ox}$ (V)	$E_{onset/Red}$ (V)	HOMO	LOMO	band gap (eV)
PF6OC6	3.09	0.87	−2.70	5.57	2.00	3.57
PF6OC8	3.09	0.93	−2.70	5.63	2.00	3.63
PF6OC10	3.09	0.94	−2.70	5.64	2.00	3.64
PF6OC12	3.09	0.94	−2.70	5.64	2.00	3.64

fwhm on the length of alkoxy side chains is probably closely related to the intermolecular interaction. In general, the intermolecular interaction in dilute solution is very weak and thus can usually be neglected. Thus, it can be concluded that the PL spectra are mainly affected by the backbone structure, which is consistent with the experimental results. However, when the samples are changed from dilute solution to film, the intermolecular interaction (i.e., aggregation) cannot be neglected. For most conjugated polymers, their spectra exhibit red shift and the corresponding fwhm increases from solution to film. Here, the intermolecular interaction mainly comes from the microphase separation between the flexible side chains and the conjugated backbones. The longer side chains can more effectively promote the microphase separation than the shorter ones. Therefore, the dependence of the vibronic structures and the fwhm on the length of alkoxy side chains can be attributed to the variation of microphase separation. Effective microphase separation can efficiently restrain the formation of aggregations among the backbones, and the vibronic structures and the fwhm decrease as the side-chain length increases.

The spectral stability of the films was investigated by annealing treatment. Figure 14 shows the PL spectra of the films annealed at 80 and 200 °C for 1 h in air. The PL spectra of the annealed films do not show a noticeable difference in spectral shape, compared with those of the pristine films (except for a very weak emission band at the long wavelength region), indicating the excellent thermal stability of the spectra. The dependence of the vibronic structures and the fwhm on the length of alkoxy side chains for the annealed films is also consistent with that for the pristine films. An additional investigation on photoluminescence quantum efficiency (PLQE) has been performed to further compare the optical properties of the polymers. PLQE measurements of the solutions are carried out with quinine sulfate as the standard material.[42] The PLQE values of the solutions and the pristine films are summarized in Table 2. The values of PLQE are about 50% and 40.0% for the solutions and the pristine films of the polymers, respectively, which do not exhibit a dependence on the length of alkoxy side chains on phenylene.

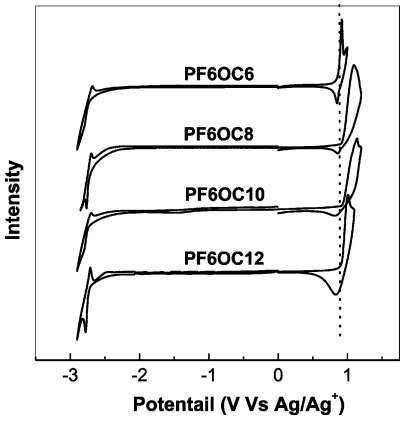

Figure 15. Cyclic voltammograms of the polymer films.

Electrochemical Properties. The band gap energies determined from the absorption onset wavelengths of the polymers are summarized in Table 3. All four polymers show similar band gaps of about 3.09 eV, also indicating that the electronic structure of the polymer backbone does not vary much with the length of alkoxy side chains on phenylene. The electrochemical behavior of the polymers was investigated using cyclic voltammetry (CV) measurements. The cyclic voltammograms are shown in Figure 15, and the corresponding data are summarized in Table 3. The CV results show that all four polymers exhibit reversibility in both n-doping and p-doping processes. The polymers show the same reduction onset potentials of about −2.70 V, and the corresponding lowest unoccupied molecular orbital (LUMO) energy levels can be estimated to be 2.00 eV, indicating no generation of new electronic state as the length of alkoxy side chains on phenylene increases. This is probably due to the uniform backbone structure of poly(fluorene-*alt*-phenylene). However, the oxidation onset potentials of the polymers slightly increase with increasing the length of alkoxy side chains. The oxidation onset potentials are 0.87, 0.93, 0.94, and 0.94 V, and the corresponding highest occupied molecular orbital (HOMO) energy levels are 5.57, 5.63, 5.64, and 5.64 eV for PF6OC6, PF6OC8, PF6OC10, and PF6OC12, respectively. The increase of HOMO energy levels may be attributed to the decrease of effective conjugation of the polymer chains arising from the steric hindrance and the microphase separation as the length of alkoxy side chains increases. The band gap energies of the polymers determined by the CV experiments are estimated to be about 3.57−3.64 eV.

Conclusions

In summary, the structural evolution and physical properties of poly(9,9-dihexylfluorene-*alt*-2,5-dialkoxybenzene) copolymers with different lengths of alkoxy side chains on phenylene have been systematically investigated. It has been found that the thermal stability of the copolymers gradually decreases with increasing the length of alkoxy side chains. The copolymers can self-organize and form a lamellar structure consisting of the interdigitated two-layer packing and the one-layer packing. The XRD results further indicate that the population of the two-

layer packing is much higher than that of the one-layer packing. In addition, the two-layer packing and the one-layer packing also accompany the presence of planar stacking and/or crystalline and noncrystalline structures, thus maintaining the stability of the packing structure. The four copolymers studied here exhibit obvious phase behavior, which is dependent on the length of alkoxy side chains on phenylene. This is attributed to the variation of the microphase separation between the alkoxy side chains and the conjugated backbones with increasing the length of alkoxy side chains. PF6OC6 shows two crystalline phases and one nematic phase during the heating process. However, PF6OC8, PF6OC10, and PF6OC12 show only one crystalline phase and one nematic phase. Also, a melting−recrystallization phenomenon during heating in DSC is steadily prohibited as the length of the alkoxy side chain increases. The vibronic structures and the fwhm gradually decrease, while the oxidation onset potentials and the corresponding HOMO energy levels slightly increase with increasing the length of alkoxy side chains on phenylene. However, the optical and electrochemical properties of the polymers do not exhibit a noticeable dependence on the length of the alkoxy side chains.

Acknowledgment. This work was financially supported by the National Natural Science Foundation of China (Grant 50403012), the "Program for New Century Excellent Talents (NCET) in University" (Grant NCET-04-0355), and the "Shanghai Rising-Star Program" (Grant 04QMX1403).

References and Notes

(1) Ohmori, Y.; Uchida, M.; Muro, K.; Yoshino, K. *Jpn. J. Appl. Phys.* **1991**, *30*, L1941.

(2) Pei, Q.; Yang, Y. *J. Am. Chem. Soc.* **1996**, *118*, 7416.

(3) Grell, M.; Bradley, D. D. C.; Inbasekaran, M.; Woo, E. P. *Adv. Mater.* **1997**, *9*, 798.

(4) Ranger, M.; Rondeau, D.; Leclerc, M. *Macromolecules* **1997**, *30*, 7686.

(5) Scherf, U.; List, E. J. W. *Adv. Mater.* **2002**, *14*, 477.

(6) Surin, M.; Hennebicq, E.; Ego, C.; Marsitzky, D.; Grimsdale, A. C.; Müllen, K.; Brédas, J. L.; Lazzaroni, R.; Leclère, P. *Chem. Mater.* **2004**, *16*, 994.

(7) Misaki, M.; Ueda, Y.; Nagamatsu, S.; Yoshida, Y.; Tanigaki, N.; Yase, K. *Macromolecules* **2004**, *37*, 6926.

(8) Rughooputh, S. D. D. V.; Nowak, M.; Hotta, S.; Heeger, A. J.; Wudl, F. *Synth. Met.* **1987**, *21*, 41.

(9) Aasmundtveit, K. E.; Samuelsen, E. J.; Guldstein, M.; Steinsland, C.; Flornes, O.; Fagermo, C.; Seeberg, T. M.; Pettersson, L. A. A.; Inganas, O.; Feidenhans'l, R.; Ferrer, S. *Macromolecules* **2000**, *33*, 3120.

(10) Babel, A.; Jenekhe, S. A. *Macromolecules* **2003**, *36*, 7759.

(11) Kline, R. J.; McGehee, M. D.; Kadnikova, E. N.; Liu, J.; Frechet, J. M.; Toney, M. F. *Macromolecules* **2005**, *38*, 3312.

(12) Teetsov, J.; Fox, M. A. *J. Mater. Chem.* **1999**, *9*, 2117.

(13) Kawana, S.; Durrell, M.; Lu, J.; Macdonald, J. E.; Grell, M.; Bradley, D. D. C.; Jukes, P. C.; Jones, R. A. L.; Bennett, S. L. *Polymer* **2002**, *43*, 1907.

(14) Leclère, P.; Hennebicq, E.; Calderone, A.; Brocorens, P.; Grimsdale, A. C.; Müllen, K.; Brédas, J. L.; Lazzaroni, R. *Prog. Polym. Sci.* **2003**, *28*, 55.

(15) Nakazawa, Y. K.; Carter, S. A.; Nothofer, H. G.; Scherf, U.; Lee, V. Y.; Miller, R. D.; Scott, J. C. *Appl. Phys. Lett.* **2002**, *80*, 3832.

(16) Tirapattur, S.; Belletete, M.; Drolet, N.; Bouchard, J.; Ranger, M.; Leclerc, M.; Durocher, G. *J. Phys. Chem. B* **2002**, *106*, 8959.

(17) Geng, Y. H.; Culligan, S. W.; Trajkovska, A.; Wallace, J. U.; Chen, S. H. *Chem. Mater.* **2003**, *15*, 542.

(18) Stepanyan, R.; Subbotin, A.; Knaapila, M.; Ikkala, O.; Brinke, G. *Macromolecules* **2003**, *36*, 3758.

(19) McCarthy, T. F.; Witteler, H.; Pakula, T.; Wegner, G. *Macromolecules* **1995**, *28*, 8350.

(20) Lauter, U.; Meyer, W. H.; Wegner, G. *Macromolecules* **1997**, *30*, 2092.

(21) Tang, H. Z.; Fujiki, M.; Motonaga, M. *Polymer* **2002**, *43*, 6213.

(22) Tanto, B.; Guba, S.; Martin, C. M.; Scherf, U.; Winokur, M. J. *Macromolecules* **2004**, *37*, 9438.

(23) Chen, S. A.; Ni, J. M. *Macromolecules* **1992**, *25*, 6081.

(24) Chen, S. H.; Chou, H. L.; Su, A. C.; Chen, S. A. *Macromolecules* **2004**, *37*, 6883.

(25) Chen, S. H.; Su, A. C.; Chen, S. A. *J. Phys. Chem. B* **2005**, *109*, 10067.

(26) Chen, S. H.; Su, A. C.; Su, C. H.; Chen, S. A. *Macromolecules* **2005**, *38*, 379.

(27) Chen, S. H.; Su, A. C.; Su, C. H.; Chen, S. A. *J. Phys. Chem. B* **2006**, *110*, 4007.

(28) Liu, B.; Yu, W. L.; Lai, Y. H.; Huang, W. *Chem. Mater.* **2001**, *13*, 1984.

(29) Zeng, G.; Yu, W. L.; Chua, S. J.; Huang, W. *Macromolecules* **2002**, *35*, 6907.

(30) Yang, G. Z.; Chen, P.; Wang, M.; Liu, T. X. *Polym. Adv. Technol.* **2006**, *17*, 544.

(31) Yang, G. Z.; Wu, M.; Lu, S.; Wang, M.; Liu, T. X.; Huang, W. *Polymer* **2006**, *47*, 4816.

(32) Ober, C. K. *Science* **2000**, *288*, 448.

(33) Prosa, T. J.; Moulton, J.; Heeger, A. J.; Winokur, M. J. *Macromolecules* **1999**, *32*, 4000.

(34) Breiby, D. W.; Samuelsen, E. J.; Groenendaal, L.; Struth, B. *J. Polym. Sci., Part B: Polym. Phys.* **2003**, *41*, 945.

(35) Knaapila, M.; Ikkala, O.; Torkkeli, M.; Jokela, K.; Serimaa, R.; Dolbnya, I. P.; Bras, W.; ten Brinke, G.; Horsburgh, L. E.; Palsson, L.-O.; Monkman, A. P. *Appl. Phys. Lett.* **2002**, *81*, 1489.

(36) Knaapila, M.; Torkkeli, M.; Jokela, K.; Kisko, K.; Horsburgh, L. E.; Palsson, L.-O.; Seeck, O. H.; Dolbnya, I. P.; Bras, W.; ten Brinke, G.; Monkman, A. P.; Ikkala, O.; Serimaa, R. *J. Appl. Crystallogr.* **2003**, *36*, 702.

(37) Futterer, T.; Hellweg, T.; Findenegg, G. H.; Frahn, J.; Schluter, A. D.; Bottcher, C. *Langmuir* **2003**, *19*, 6537.

(38) Knaapila, M.; Stepanyan, R.; Lyons, B. P.; Torkkeli, M.; Monkman, A. P. *Adv. Funct. Mater.* **2006**, *16*, 599.

(39) Samuelsen, E. J.; Mardalen, J. In *Handbook of Organic Conductive Molecules*; Nalwa, H. S., Ed.; Wiley: New York, 1997; p 87.

(40) Wang, W.; Lieser, G.; Wegner, G. *Macromolecules* **1994**, *27*, 1027.

(41) Ballauff, M. *Angew. Chem., Int. Ed.* **1989**, *28*, 253.

(42) Huang, C. H.; Li, F. Y.; Huang, Y. Y. *Ultrathin Films for Optics and Electronics*; Beijing University Press: Beijing, 2001.